Journal of Alloys and Compounds 792 (2019) 203–214

Contents lists available at ScienceDirect

Journal of Alloys and Compounds

journal homepage: http://www.elsevier.com/locate/jalcom

AlSi10Mg alloy nanocomposites reinforced with aluminum-coated graphene: Selective laser melting, interfacial microstructure and property analysis

Zhanyong Zhao [a], Peikang Bai [a, **], R.D.K. Misra [b, ***], Mengyao Dong [e, f], Renguo Guan [c], Yanjun Li [d], Jiaoxia Zhang [e, h], Le Tan [a], Jianfeng Gao [a], Tao Ding [g, ****], Wenbo Du [i], Zhanhu Guo [e, *]

[a] School of Materials Science and Engineering, North University of China, Taiyuan 030051, China
[b] Department of Metallurgical and Materials Engineering, 500 W. University Avenue, University of Texas at El Paso, TX 79968, USA
[c] School of Materials Science and Engineering, Northwestern Polytechnical University, Xi'an 710072, China
[d] Department of Materials Science and Engineering, Norwegian University of Science and Technology, Alfred Getz vei 2 B, N-7491 Trondheim, Norway
[e] Integrated Composites Laboratory, Department of Chemical and Biomolecular Engineering, University of Tennessee, Knoxville, TN 37996, USA
[f] Key Laboratory of Materials Processing and Mold (Zhengzhou University), Ministry of Education, National Engineering Research Center for Advanced Polymer Processing Technology, Zhengzhou University, Zhengzhou 450002, China
[g] College of Chemistry and Chemical Engineering, Henan University, Kaifeng 475004, China
[h] School of Material Science and Engineering, Jiangsu University of Science and Technology, Zhenjiang, Jiangsu, 212003, China
[i] National Key Laboratory for Remanufacturing, Academy of Army Armored Forces, China

ARTICLE INFO

Article history:
Received 17 February 2019
Received in revised form
30 March 2019
Accepted 1 April 2019
Available online 3 April 2019

Keywords:
Graphene
Al nanocoating
AlSi10Mg alloy
Selective laser melting
Microstructure
Property

ABSTRACT

Graphene has been successfully coated with a nano-Al layer through a novel activating treatment (i.e., organic aluminum reduction method). The nano-Al coated graphene was further processed into AlSi10Mg alloy based composites through a selective laser melting (SLM) process. During the nano-coating of Al on graphene, Al atoms deposited on the graphene through organic aluminum reduction gradually, via nucleation and growth process. There were two primary grain growth patterns: two dimensional (2D) layered growth and three dimensional (3D) island growth, until graphene was coated with Al. The Al-coated graphene was added to the AlSi10Mg alloy, refining the cell, increased the tensile strength, hardness and wear resistance of the alloy. Coating Al on the graphene improved the wetting between graphene and Al, and the addition of Al-coated graphene led to a high nucleation rate, which was responsible for refining the cell. This approach facilitated graphene homogeneous distribution in the Al alloy, the interface between graphene and Al was relatively stable, and the grapheme could pin the dislocation and grain boundary. All these attributes enabled superior mechanical properties to be obtained in the final alloy based nanocomposites.

1. Introduction

With high toughness, high conductivity and high strength [1–5], graphene or reduced graphene oxide have been used for many applications including energy storage/conversion [6–9], electromagnetic interference (EMI) shielding [10,11], sensors [12–14], and one additional unique field of preparing reinforced metal (such as Al) composites for wide applications in situations where excellent properties in mechanics, photology, electricity and thermology are required [15–17]. The main methods to prepare graphene/Al composites include liquid stir casting, friction stir processing, ball milling and hot extrusion, cryomilling and powder metallurgy. For example, Guan et al. prepared Al-graphene composites and Mg matrix composites with high strength via liquid stir casting and rheo-rolling [18–20]. Graphene/Al matrix composites with enhanced thermal conductivity were fabricated by friction stir

* Corresponding author.
** Corresponding author.
*** Corresponding author.
**** Corresponding author.
E-mail addresses: baipeikang@nuc.edu.cn (P. Bai), dmisra2@utep.edu (R.D.K. Misra), zguo10@utk.edu (Z. Guo).

https://doi.org/10.1016/j.jallcom.2019.04.007
0925-8388/

processing method [21]. Zhang and Li et al. successfully fabricated graphene/Al composites by ball milling and hot extrusion [22,23]. While Yan et al. investigated Al-3.9Cu-1.5 Mg alloys reinforced by graphene nanoflakes via powder metallurgy [24]. Complex shaped parts are difficult to be produced with these forming methods. Both poor wettability and density difference between graphene and Al cause easy agglomeration of graphene in the Al matrix, to obtain homogeneous distribution of graphene in metals is still a challenge [25–28].

Selective laser melting (SLM) could be used to quickly prepare complex parts, through selectively melting successive layers of powders by the laser beam [29–33]. For example, Song et al. prepared Cr_3C_2/Fe nanocomposites with excellent tensile properties and hardness using the SLM process [34]. Simchi et al. found that the graphite promoted the quality of parts prepared by laser sintering [35]. Attar et al. prepared porous Ti-TiB composites by SLM and studied the mechanical behavior of porous Ti-TiB composite materials [36]. Gu et al. demonstrated that the SLM method could produce Ti-based bulk nanocomposites with excellent wear resistance [37]. Hu et al. reported that the graphene/aluminum composites prepared by 3D printing exhibited a higher Vickers hardness. Compared with pure aluminum counterpart, the Vickers hardness for the prepared composite samples was increased by 75.3% [38]. The characteristics of SLM powders directly affected the stability of the SLM process and the properties of parts. The SLM process has very strict requirements for chemical compositions and physical properties of the powders including high purity, high sphericity, flowability and narrow size distribution (Al powder: 15–50 μm) [39].

Prior to the processing of graphene/Al composites by the SLM process, it is important to prepare graphene/Al composite powders with homogeneous distribution of graphene [38]. Because of poor wettability between Al and graphene, graphene is easy to accumulate in the Al powders. Activating treatment can improve the wettability between graphene and Al, and the metal coating on a graphene surface is one of the most important activating treatments. Many methods for coating metal on graphene surfaces have been reported such as electrochemical deposition, self-assembly, chemical reduction, redox method, and vapor deposition. For example, Muszynski et al. decorated graphene sheets with gold nanoparticles [40]. Hong et al. prepared gold-coated graphene by self-assembly [41]. Luo et al. potentiostatically electrodeposited Cu nanoparticles on graphene sheets [42]. However, precious metals such as copper or nickel in Al powders are thought to be impurities, and can affect the laser absorptivity of powders during the SLM processing [43,44]. Coating Al on the graphene is an effective method to reduce these impurities. However, it is difficult to coat Al on the graphene through the conventional Al salt solution reaction because of active nature of Al [45,46]. Organic aluminum reduction method to coat nano-coat Al on graphene was reported. The effects of reaction temperature and reducing agent were studied and high quality Al-coated graphene was obtained [45,46]. However, to use the Al coated graphene for making AlSi10Mg alloy nanocomposites has not been reported yet.

In this study, the nano-Al coated graphene was further processed into graphene/Al composite powders with homogeneous distribution of graphene by vacuum ball milling. The Al-coated graphene powders and Al powders at different ratios were fabricated into AlSi10Mg alloy nanocomposites through SLM. The tensile strength, hardness and wear resistance of the alloy were studied. Meanwhile, the formation mechanism of Al coating, as well as the microstructure and mechanical properties of the Al-coated graphene AlSi10Mg alloy composites prepared by SLM were studied. The graphene AlSi10Mg alloy composites were also prepared and their properties were studied for comparison.

2. Experimental method

2.1. Nano-Al coating on graphene

Graphene (Fig. 1a) and AlSi10Mg powders (an average size of 15–50 μm, Fig. 1b) were supplied by Tangshan Jianhua Science and Technology Development Co., Ltd., and China and Renishaw Plc. UK, respectively.

Organic aluminum chemical reduction was used to coat Al on the graphene. First, the alkyl aluminum solution was prepared. Using sodium metal wire as an indicator, 1.49 g Al powders (Hunan crest Technology Co., Ltd., China), 29 mL bromoethane (Tianjin Da Mao chemical reagents factory, China), 0.1 g iodine (Tianjin Da Mao chemical reagents factory, China) and 0.1 g aluminum chloride (Tianjin Da Mao chemical reagents factory, China) were placed in a reaction vessel filled with hydrogen. The reaction solution protected by H_2 was stirred at 39 °C. When the color of the solution did not change, the reaction temperature was decreased and held for 1 h at 0 °C. Subsequently, tetrahydrofuran (4 mL) was added into the vessel. The solution was filtered when the reaction was completely over, and the alkyl aluminum solution was formed. Secondly, the alkyl aluminum solution was heated at 70 °C. 0.05 g graphene was added into alkyl aluminum solution protected by H_2 and stirred. After reacting for 2 h, the Al was coated on the graphene.

The Al-coated graphene and AlSi10Mg powders were ball milled with a QM-3SP4 ball mill (Nanjing University Capital Management Co., Ltd., Jiangsu, China) for 2 h in a vacuum. The mass ratio of powders to balls was 1:8 w/w, and the speed was 230 rpm. During the process, the stainless steel balls with a 5 mm diameter were used. Finally, the Al-coated graphene/AlSi10Mg composite powder with the homogeneous distribution of graphene was prepared. The

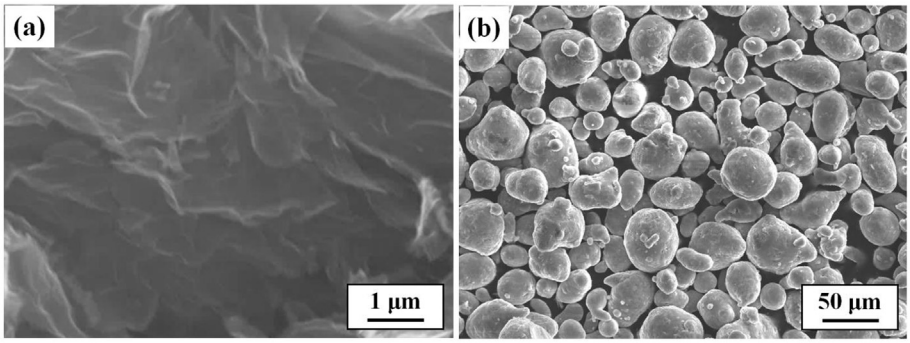

Fig. 1. SEM observations show the morphologies of (a) graphene, and (b) AlSi10Mg powers.

content of graphene was 1 wt%. In order to study the effects of coating Al on graphene, the graphene (without coating Al)/AlSi10Mg powders were prepared by ball milling process.

2.2. SLM process

The Renishaw AM400 machine (AM400, Renishaw) used was an Yb fiber laser (wavelength 1070 nm). The laser power was 200–400 W, the hatch spacing was 130 μm, scanning speed was 1200 mm/s, and the exposure time was 100–160 μs. A chessboard laser-scan strategy was used, and the hatching was rotated by 67° in each layer prior to the next exposure. The powder layer thickness was 30 μm, and the building platform was heated to 180 °C before SLM processing. The SLM process was under argon protection, and the oxygen was less than 0.1%. The Al-coated graphene/AlSi10Mg composites as well as graphene (without coating Al)/AlSi10Mg composites were prepared by SLM as well for comparison.

2.3. Microstructural observation

The samples were polished and etched via a solution of 2.5 vol% HNO_3+1 vol%HF+95 vol% H_2O+1.5 vol%HCl. Microstructure observation was carried out using a scanning electron microscope (SEM) equipped with energy dispersive spectroscopy (EDS) (Zeiss Ultra 55, Jena, Germany). The precipitates in the Al-coated graphene reinforced Al matrix composites was analyzed by X-ray diffraction (XRD) (X'Pert, Almelo, Holland). The specimens for TEM observations were cut from the samples, and was ground to 80 μm. The specimens were further thinned with Gatan 691 ion polishing system. High-resolution transmission electron microscopy (HRTEM, Tecnai G2 F20, FEI, USA) was used to perform TEM inspections.

2.4. Mechanical and wear behavior

The densities of Al-coated graphene/AlSi10Mg composite were measured using Archimedes' method [47]. The mechanical properties of the composites were evaluated using an MTS 810 mechanical properties testing system (MTS, USA). The strain rate was 5×10^{-3} s^{-1} at room temperature. At least three tensile tests were performed to ensure repeatability and accuracy of the data. Fig. 2 shows the geometry and dimensions of the tensile specimens. The hardness was measured via a Vickers hardness tester (TMHVS-1000, Beijing Shidai Shanfeng Technology CO., LTD, China) at a load of 1.96 N for 15 s. Friction and wear tests were carried out on MFT-4000 friction and wear testing machine (Lanzhou Huahui Instrument Technology Co., Ltd., China). The module did a linear reciprocating motion (room temperature) at a load of 20 N, the friction distance was 5 mm, the frequency was 100 mm/min and the wear time was 20 min. The friction pair was A GCr15 steel, the hardness was 65 HRC, and the diameter was 4 mm.

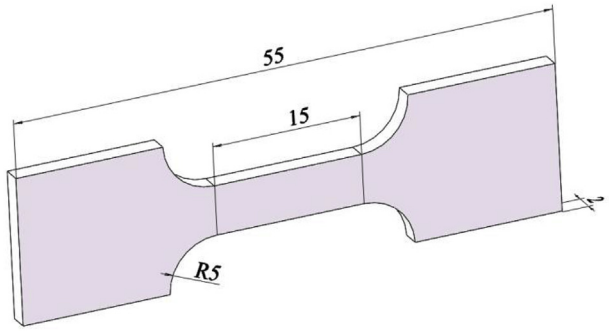

Fig. 2. Configuration of the samples used for the tensile tests (unit:mm).

3. Results and discussion

3.1. The Al-coated graphene

The morphology and composition of Al-coated graphene are

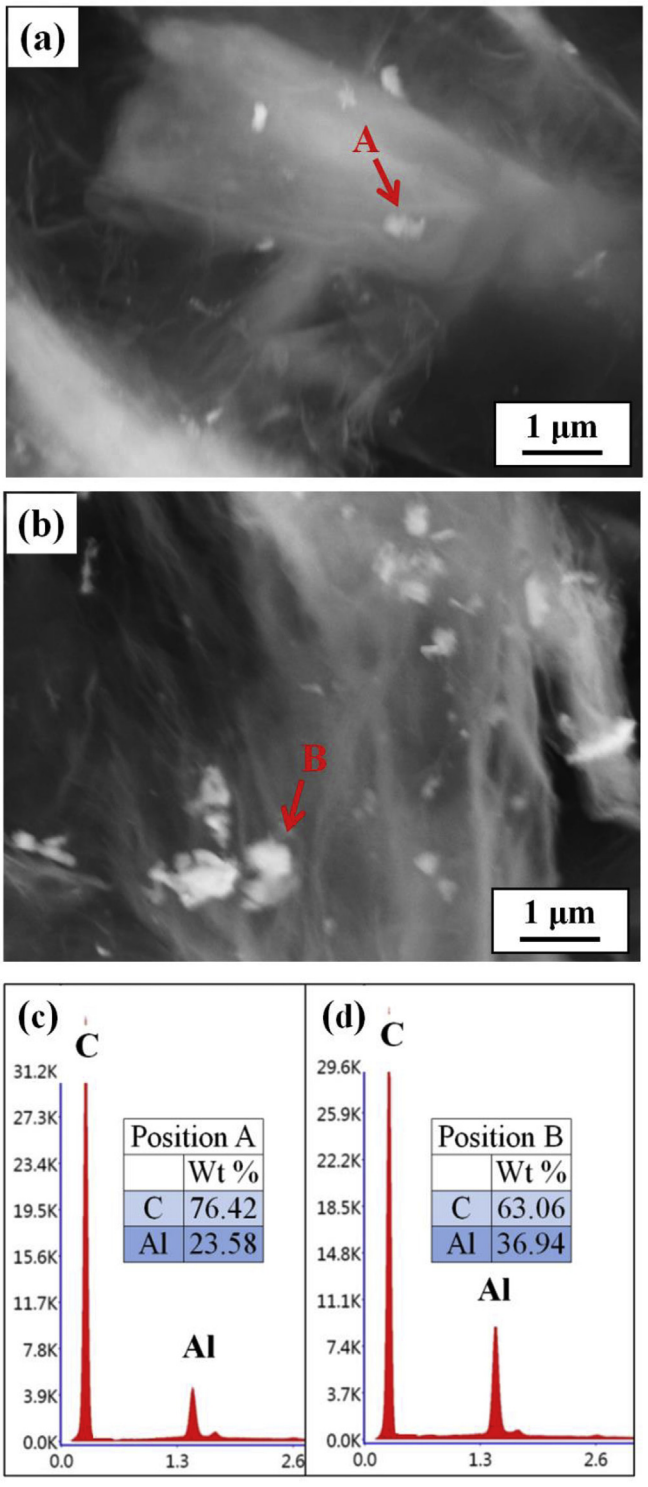

Fig. 3. SEM microstructures of Al-coated graphene with a reaction time of (a) 0.5, (b) 1.0 h; (c) and (d) EDS spectra of the corresponding sample.

shown in Fig. 3. The graphene maintained its irregular curls and folds, indicating that mechanical stirring did not affect the structure of graphene. After reacting for 0.5 h, there were a few particles in small local areas of graphene surface. Based on XRD and EDS analyses (Figs. 3 and 4), the heterogeneous particles on the graphene surface were determined to be Al particles. The diffraction peaks of Al phase were weaker (Fig. 4). With increasing the reaction time, the volume fraction of Al particles on graphene was increased (Fig. 3b and c). When the reacting time reached 1.5 h (Fig. 5), the diffraction peaks corresponding to the Al phase became increased and sharper, indicating a larger size of the particles, as shown in Fig. 5 (point c and d). Most Al particles were homogeneously coated on the graphene (Fig. 5), and the content of Al element was 71% (Fig. 5e). The Al-coated graphene was successfully prepared.

The HRTEM images of Al particles coating on the graphene are shown in Fig. 6. When the reaction time was 0.5 h, a few particles with crystal structures were formed on the graphene and distributed discontinuously. These particles were identified from the HRTEM micrograph to have [1 1 0] orientation (Fig. 6a). As the reaction continued, lots of Al particles nucleated gradually and grew up, and the dispersed Al particles gradually became segregated (Fig. 6b) and coated evenly on the graphene (Figs. 5 and 6). During the reaction process, there were two kinds of Al coating surface, one was smooth (Fig. 7a), and the other had an island structure (Fig. 7b).

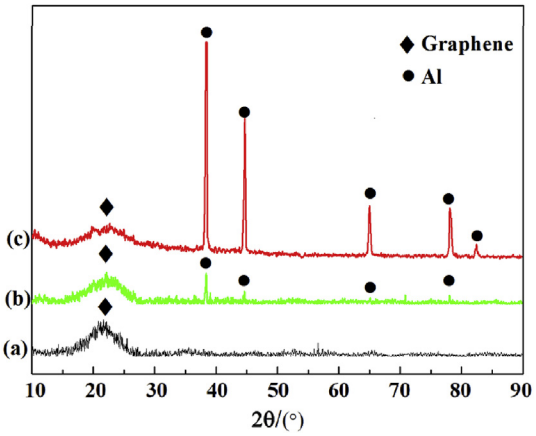

Fig. 4. XRD patterns for Al-coated graphene with a reaction time of (a) 0, (b) 0.5, and (c) 1.0 h.

Coating Al on the graphene could be divided into two steps. The first was the preparation in the alkyl aluminum solution. While the second step was a gradual deposition on the surface of graphene with the decomposition of alkyl aluminum. After the Al powders were added into the C_2H_5Br solution, the reaction between C_2H_5Br and Al powders led to $(C_2H_5)_2AlBr$ and $C_2H_5AlBr_2$, following Equation (1):

$$3C_2H_5Br + 2Al \rightarrow (C_2H_5)_2AlBr + C_2H_5AlBr_2 \quad (1)$$

The product from the reaction between $C_2H_5AlBr_2$ and Al powders further reacted to produce $(C_2H_5)_2AlBr$ following Equation (2):

$$2C_2H_5AlBr_2 + Al \rightarrow (C_2H_5)_2AlBr + Al + AlBr_3 \quad (2)$$

The $(C_2H_5)_2AlBr$ reacted with Al to produce $(C_2H_5)_3Al$, new Al and $AlBr_3$ following Equation (3):

$$3(C_2H_5)_2AlBr + Al \rightarrow 2(C_2H_5)_3Al + Al + AlBr_3 \quad (3)$$

The $(C_2H_5)_3Al$ has a poor thermal stability and can be easily decomposed at high temperatures. With mechanical stirring, the $(C_2H_5)_3Al$ was dispersed homogeneously on the surface of graphene and decomposed gradually into $(C_2H_5)_2AlH$ and C_2H_4 following Equation (4):

$$(C_2H_5)_3Al \rightarrow (C_2H_5)_2AlH + C_2H_4 \quad (4)$$

When C_2H_4 was formed, C_2H_4 reacted with $(C_2H_5)_3Al$ to produce

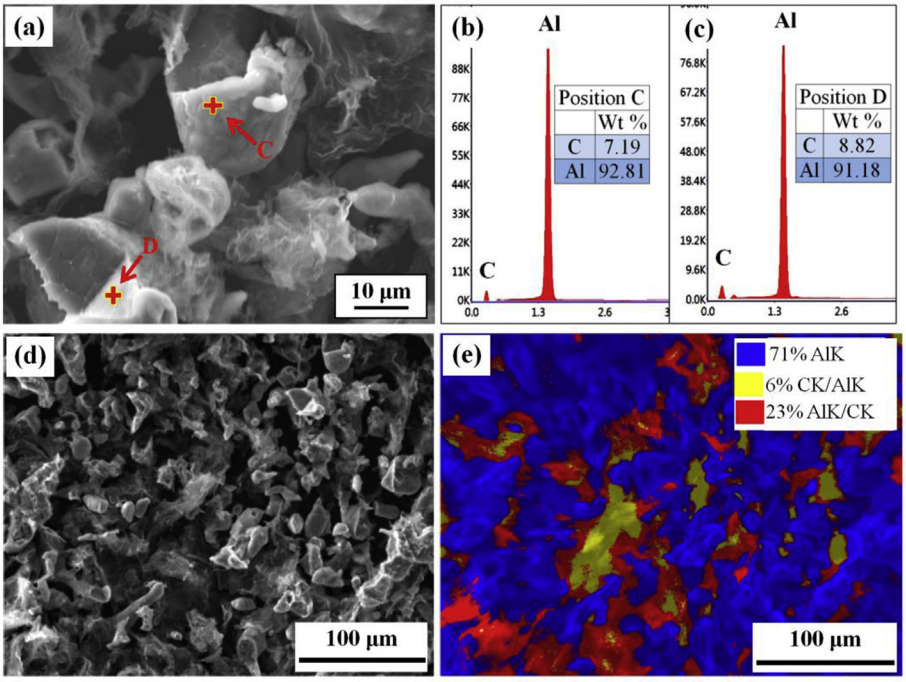

Fig. 5. SEM microstructures of (a, d) Al-coated graphene, (b, c) composition analysis at point C and D, (e) Al and C distribution maps of Al-coated graphene. The coating time was 1.5 h.

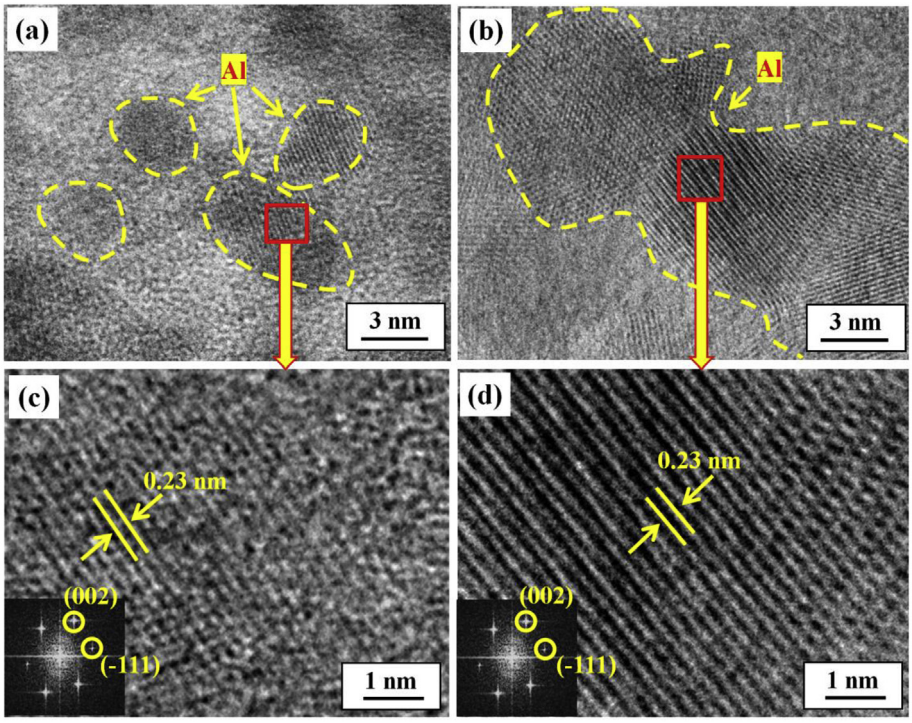

Fig. 6. High-resolution TEM images of the Al-coated graphene with a reaction time of (a, c) 0.5, and (b, d) 1 h.

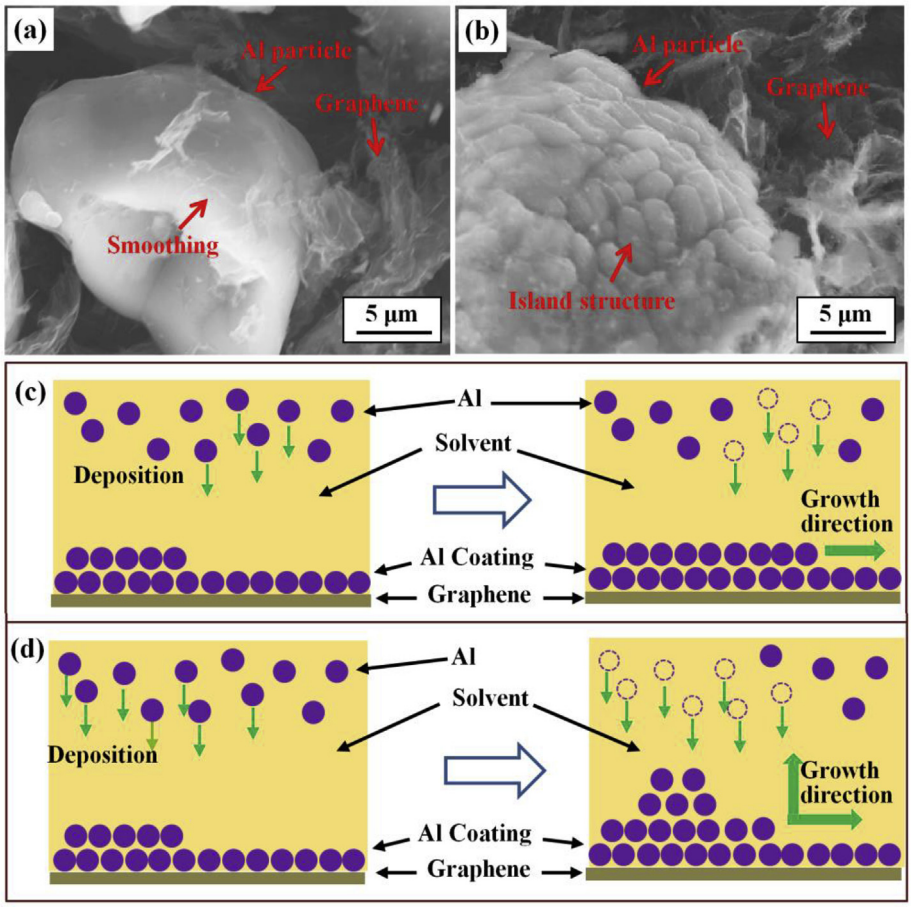

Fig. 7. The Al coating surface (a, b), the schematic illustration indicates the Al particles with a two dimensional (2D) layered growth (c) and three dimensional (3D) island growth (d).

$(C_2H_5)_2AlCH_2C_2H_5$, following Equation (5):

$$(C_2H_5)_3Al + CH_2 = CH_2 \rightarrow (C_2H_5)_2AlCH_2CH_2C_2H_5 \quad (5)$$

When the $(C_2H_5)_2AlCH_2C_2H_5$ was formed, the $(C_2H_5)_2AlCH_2C_2H_5$ reacted with C_2H_4 to produce $(C_2H_5)_3Al$ and $CH(C_2H_5) = CH_2$ following Equation (6):

$$(C_2H_5)_2AlCH_2CH_2C_2H_5 + CH_2 = CH_2 \rightarrow (C_2H_5)_3Al + CH(C_2H_5) = CH_2 \quad (6)$$

On the other hand, the $(C_2H_5)_2AlCH_2C_2H_5$ was decomposed gradually into $(C_2H_5)_2AlH$ and $C_2H_5CH = CH_2$ following Equation (7):

$$(C_2H_5)_2AlCH_2CH_2C_2H_5 \rightarrow (C_2H_5)_2AlH + C_2H_5CH = CH_2 \quad (7)$$

The $(C_2H_5)_2AlH$ was further decomposed into Al, H_2 and C_2H_4 following Equation (8):

$$(C_2H_5)_2AlH \rightarrow Al + \frac{3}{2}H_2 + 2C_2H_4 \quad (8)$$

In summary, the reaction formula of thermal decomposition of $(C_2H_5)_3Al$ can be summarized as:

$$2(C_2H_5)_3Al \rightarrow 6C_2H_4 + 3H_2 + 2Al \quad (9)$$

The Al particles were gradually built up on graphene with the decomposition of $(C_2H_5)_3Al$. With the reaction processing, lots of Al particles were nucleated gradually and grew up, and the dispersed Al particles were gradually accumulated (Fig. 6) and coated homogeneously on the graphene (Fig. 5).

After the Al particles were nucleated on the graphene surface, there were two primary grain growth patterns: two dimensional (2D) layered growth and three dimensional (3D) island growth. The two dimensional layered growth involved the layer-by-layer growth, while maintaining the two-dimensional (2D) morphology of Al coated surface, and the Al coated surface was smooth, as shown in Fig. 7a. During the reaction process, the Al atoms in the solution gradually built up on the graphene to form an Al coated layer, a region of low concentration of Al atoms was formed above the coated layer, which hindered the growth of Al coated layer normal to the coated surface direction. Thus, the coated layer preferentially grew along the horizontal direction (Fig. 7c). After the formation of a layer or multilayer Al atomic layer on the surface of the graphene, the low concentration area of Al atoms was constantly destroyed by mechanical stirring. The Al atoms continued to deposit on the coating, and the next Al coated layer was formed by two-dimensional (2D) layered growth. Besides the 2D layered growth pattern, three dimensional (3D) island growth could also occur, the Al coated surface had an island structure, as shown in Fig. 7b. The $(C_2H_5)_3Al$ was decomposed into Al, H_2 and C_2H_4 during the reaction. The H_2 and C_2H_4 floated on the surface and destroyed the local Al low concentration region, such that the Al atoms were continuously deposited on the coated layer normal to the coated direction, making the coating grow along the normal direction of the coated surface, while at the same time, the coated layer grew along the horizontal direction (Fig. 7d). Therefore, the Al coated layer was formed by the three dimensional (3D) island growth.

3.2. The microstructure and properties of Al-coated graphene/AlSi10Mg composites prepared by SLM

The Al-coated graphene and AlSi10Mg powders were ball milled for 2 h in vacuum. The Al-coated graphene/AlSi10Mg composite powders for SLM were prepared, as shown in Fig. 8. It was found that the Al-coated graphene was evenly dispersed in the AlSi10Mg powders. It is reported that the metal coating on a graphene surface could improve the wettability between the metal and the graphene [40–42]. Based on previous studies, we can conclude that coating Al on the graphene improved the wettability between Al and grapheme, which was beneficial for obtaining more homogeneously Al-coated graphene/AlSi10Mg composite powders. However, the effect of ball milling on the morphology of the AlSi10Mg powders was not obvious, which was beneficial to the SLM process.

Fig. 9 shows the Al-coated graphene/AlSi10Mg, graphene/

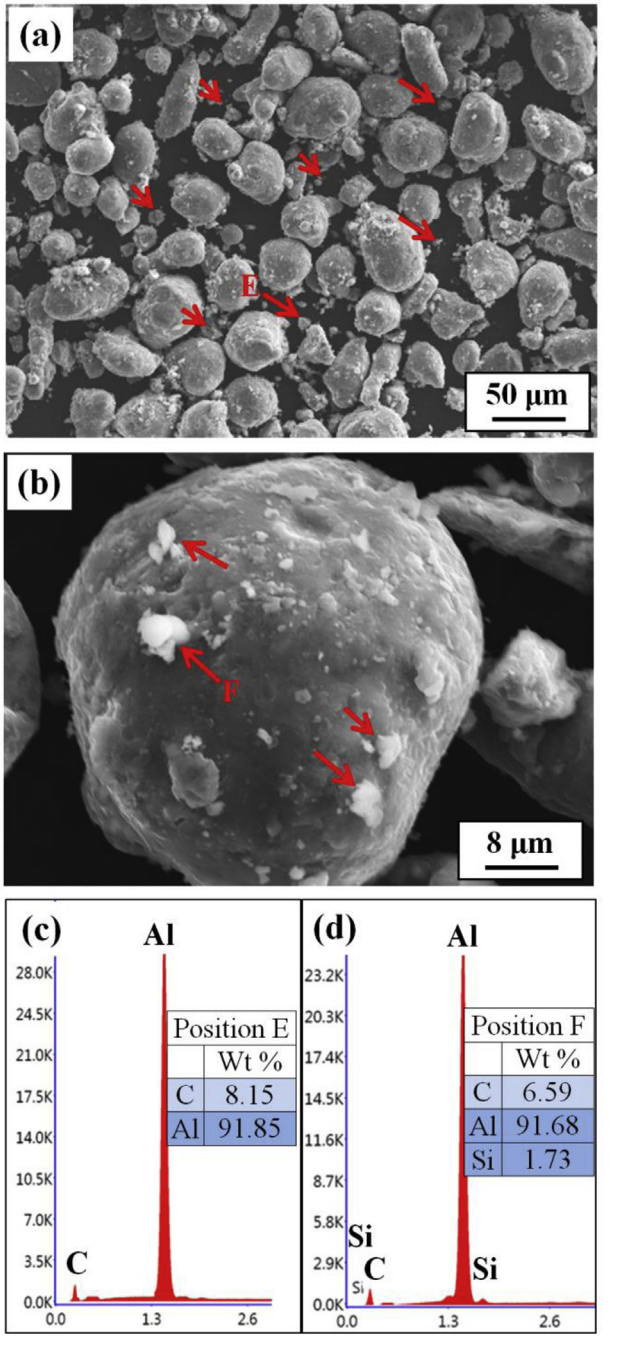

Fig. 8. SEM microstrucures of (a, b) Al-coated graphene/AlSi10Mg composite powders, (c, d) composition analysis at point E and F.

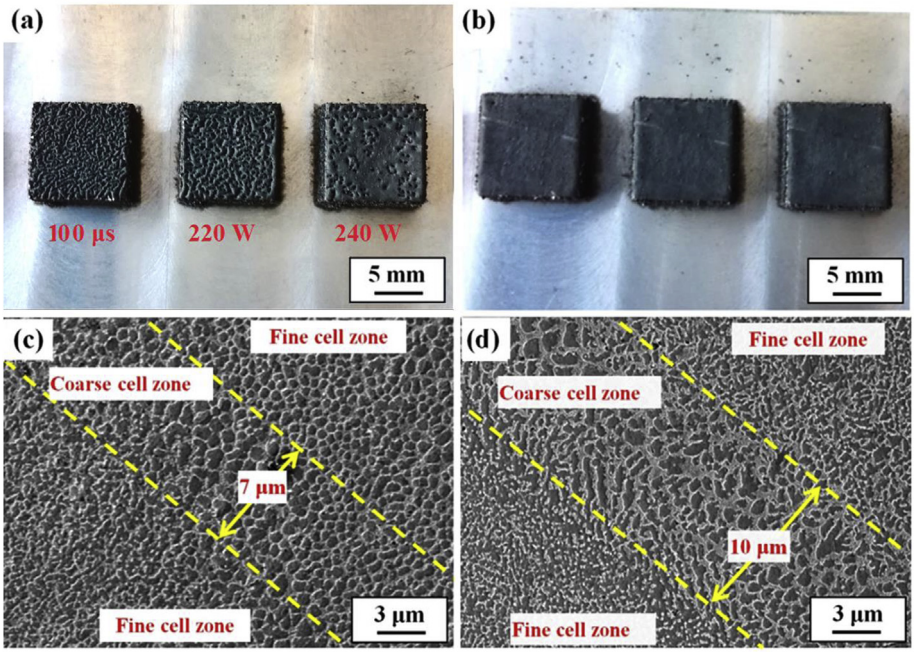

Fig. 9. Al-coated graphene/AlSi10Mg composites prepared by SLM different exposure time (100 μs) and laser power (220 W, 240 W) (a), Al-coated graphene/AlSi10Mg composites prepared by SLM exposure time 140 μs and laser power 300 W(b), the microstructure of Al-coated graphene/AlSi10Mg composites (cross section) prepared by SLM (c), the microstructure of AlSi10Mg alloy (cross section) prepared by SLM (d).

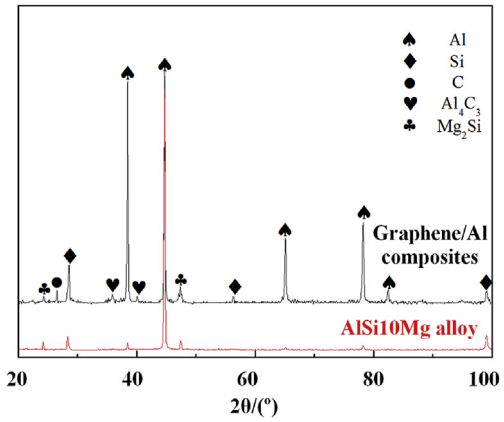

Fig. 10. XRD patterns for Al-coated graphene reinforced AlSi10Mg nanocomposites.

AlSi10Mg composites, and the AlSi10Mg alloy prepared via the SLM process and the microstructure (cross section). When the laser power was lower such as 300 W, and the exposure time was less such as 140 μs, there were lots of pores on the surface of sample, and the molten track was discontinuous (Fig. 9a), which weakened the mechanical performance of the composites. When the laser power was 300 W, and the exposure time was 140 μs, no obvious defects were observed in metals (Fig. 9b), and the relative density of the fabricated samples could reach 98%. Fine cells and coarse cell regions were observed in the prepared alloy. The fine cell region was mainly composed of equiaxed cells, and there were numbers of cellular dendrites in the coarse cell region. When the Al-coated graphene was added to the AlSi10Mg alloy, the number of coarse cells was decreased, and more fine spherical cells were formed (Fig. 9 c and d).

The phase compositions of α-Al, Si, C, Al_4C_3 and Mg_2Si in the Al-coated graphene/AlSi10Mg composites are shown in Fig. 10. The

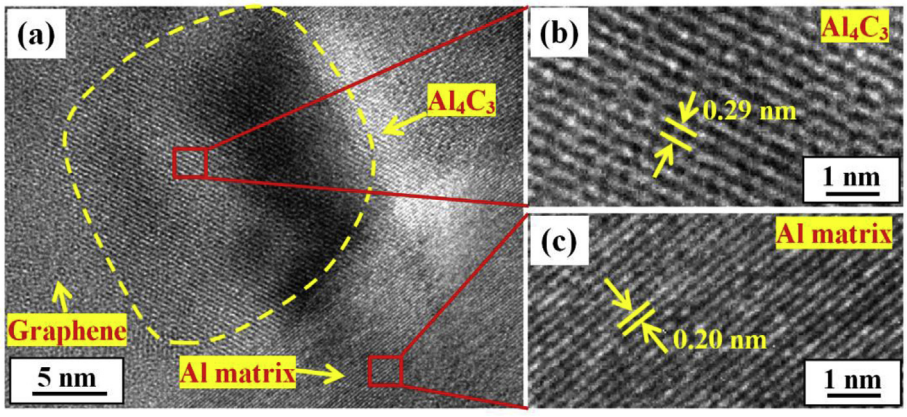

Fig. 11. High-resolution TEM images the interfacial microstructure between graphene and AlSi10Mg matrix.

eutectic Si phase appeared near the grain boundary of α-Al (Fig. 9). However, there were less Al_4C_3 and Mg_2Si (Fig. 10). The Al_4C_3 phase precipitated in the Al-coated graphene/AlSi10Mg composites, indicating the reaction of Al with graphene during the SLM process. Fig. 11 shows the interfacial microstructure between graphene and Al matrix. Aluminum carbide was also noted. Based on XRD and HRTEM analyses, the aluminum carbide near the interface between graphene and Al matrix was determined to be Al_4C_3 phase, and was nano size. Hu et al. also found similar scenario [38].

The fine particles could be seen in the composites (indicated by arrows in Fig. 12a). EDS analysis revealed that the chemical composition of that the fine particles mainly contained C, indicating that the fine particles were Al-coated graphene (Fig. 12b). The Al-coated graphene and Si were homogeneously distributed within the matrix, as shown in Fig. 9c and d. However, there were more pores in the graphene/AlSi10Mg nanocomposites, the graphene powders were severely agglomerated (Fig. 12 e and f), which resulted in a decreased strength of the alloy.

The Al-coated graphene/AlSi10Mg composites prepared by SLM exhibited a tensile strength of 396 MPa and an elongation at break of 6.2%, which was 11% and 13% higher than the AlSi10Mg alloy (357 MPa, 5.5%) prepared by SLM (Fig. 13). The hardness of Al-coated graphene/AlSi10Mg composites prepared by SLM was 169 HV, which was 40.8% higher than the AlSi10Mg alloy (120 HV) prepared by SLM. The wear resistance of Al-coated graphene/AlSi10Mg composites was better than the AlSi10Mg alloy prepared by the SLM process. After friction and wear for 20 min, the average friction coefficient of the Al-coated graphene/AlSi10Mg composites was 0.274, which was lower than the AlSi10Mg alloy (0.472) prepared via the SLM process, and the friction coefficient curve of Al-coated graphene/AlSi10Mg composites was more flat (Fig. 14). The worn surfaces of AlSi10Mg and Al-coated graphene/AlSi10Mg composites prepared by SLM after friction and wear are shown in Fig. 15. It can be seen that grooves, partial irregular pits and intense

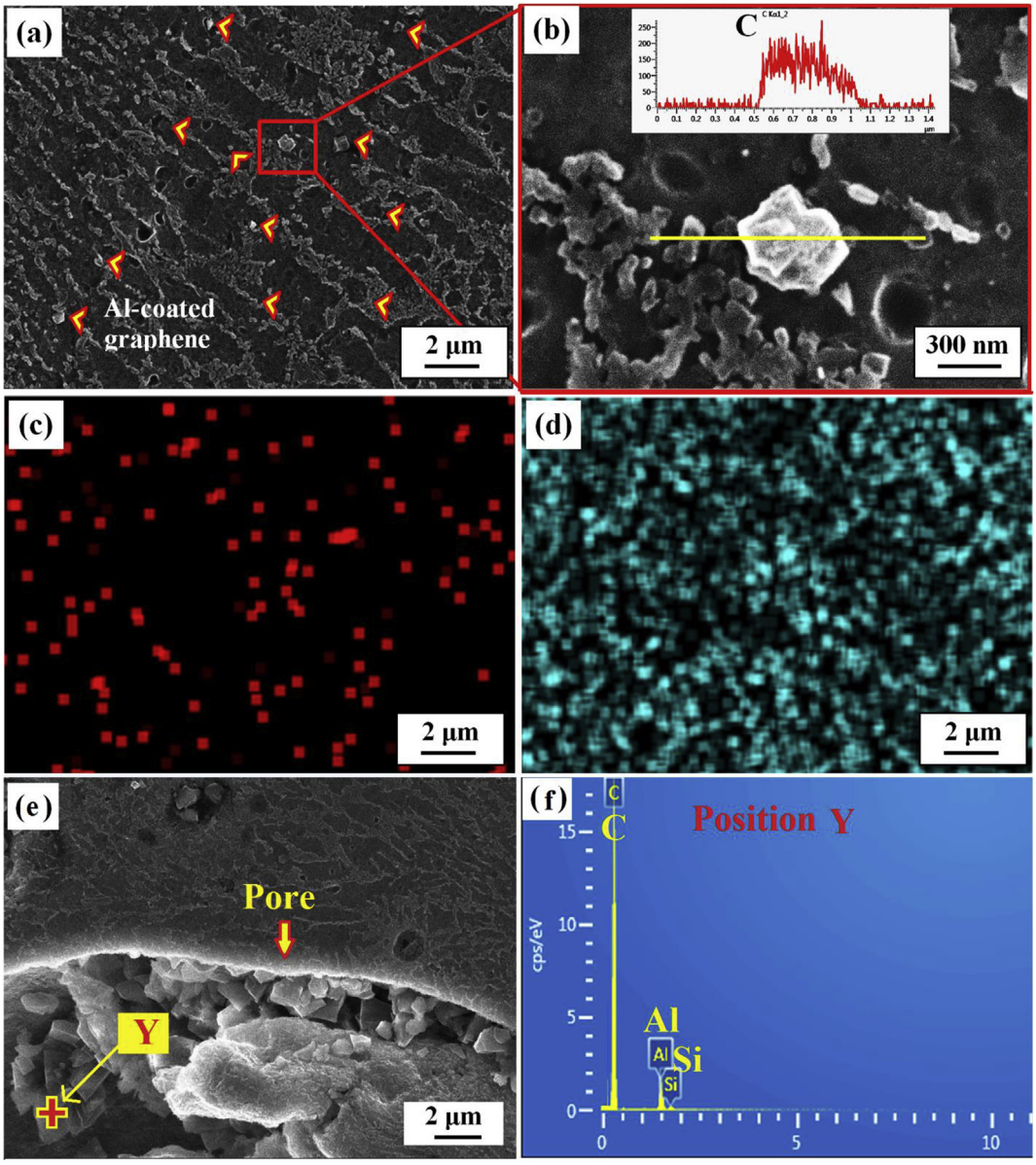

Fig. 12. SEM microstructures of composites, (a, b) Al-coated graphene/AlSi10Mg, (c) C and (d) Si distribution maps of Al-coated graphene, (e) graphene/AlSi10Mg, (f) composition analysis at point Y.

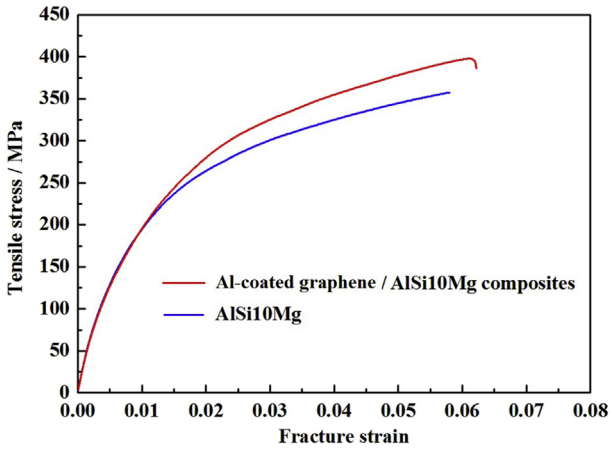

Fig. 13. Engineering stress-strain curves for AlSi10Mg alloy and Al-coated graphene/AlSi10Mg composites.

plastic deformation appeared on the worn surfaces of AlSi10Mg alloys, which indicated an adhesive wear behavior (Fig. 15a). The presence of grooves indicates the micro-cutting and micro-ploughing effect of the counter face. The adhesion occurred under experimental conditions induced a substantial attractive force between the mating surfaces, leading to a high mutual solubility of aluminum and iron. The addition of Al-coated graphene into the AlSi10Mg alloy improved the wear resistance of the composites. The grooves, partial irregular pits and intense plastic deformation were decreased in the Al-coated graphene/AlSi10Mg composites, which exhibited a self-lubricating phenomenon (Fig. 15b). The main lubrication action of the Al-coated graphene/AlSi10Mg composite was attributed to the uniformly distributed graphene in the composites, which was beneficial for obtaining good wear resistance.

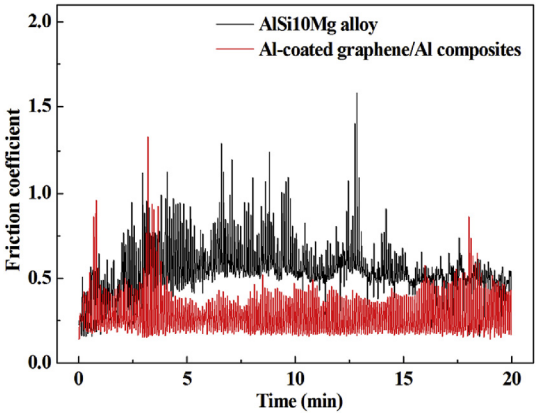

Fig. 14. The curve of friction coefficient and time.

Both fine grain and coarse cell region were observed in the AlSi10Mg alloy composites reinforced with Al-coated graphene prepared by the SLM process. During this process, laser generally provided high heating/cooling rates of molten pool, the cooling rate could reach 10^4–10^5 K/s, which was significantly higher than the melt during conventional casting and thus resulted in the nucleation and formation of a fine cell region [48]. When the next layer of AlSi10Mg powders was melted, the molten pool could directionally heat the solidified layer, making the fine cell in the solidified layer grow further, leading to the formation of a coarse cell region [49].

When the Al-coated graphene was added to the AlSi10Mg alloy, the cells were gradually refined (Fig. 9) through the following two possible mechanisms.

(i) Coating Al on the graphene improved the wetting between graphene and Al, which increased the nucleation rate.

The contact angle was obtained by Young's equation as shown by Equation (10):

$$\cos\theta = \frac{\gamma_{SG} - \gamma_{SL}}{\gamma_{LG}} \tag{10}$$

where θ is the contact angle, the γ_{SG} is the solid–vapor interfacial energy, the γ_{SL} is solid–liquid interfacial energy, and the γ_{LG} is the liquid–vapor interfacial energy [21,29].

The contact angle is related to the work of adhesion via the Young-Dupré equation as shown in Equation (10):

$$\Delta W_{SLV} = \gamma_{LG}(1 + \cos\theta) \tag{11}$$

where $\triangle W_{SLV}$ is the solid-liquid adhesion energy per unit area in the medium V. A lower contact angle is indicative of good wetting. The surface free energy of graphene was 46.7 mJ m^{-2} at room temperature [21,29]. When graphene was coated with Al, the contact angle between metal and graphene was decreased, and the wetting was increased.

(ii) During the molten pool solidification, the grain growth pattern depended on the temperature gradient and cooling rates near the solid-liquid interface. The cell size decreased with increasing the cooling rate and temperature gradient. The thermal conductivity of graphene near the solidified interface was high, which increased the cooling rate of the

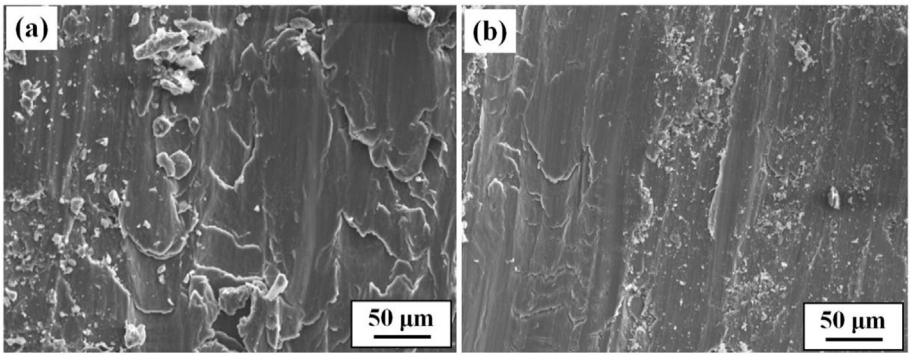

Fig. 15. SEM microstrucures of (a) AlSi10Mg alloy prepared by SLM after friction and wear, (b) Al-coated graphene/AlSi10Mg composites prepared by SLM after friction and wear.

alloy and was favorable for the formation of fine cell. The graphene was gathered near the solid-liquid interface and hindered the diffusion of the solute, which caused the homogeneous solute distribution and the formation of fine cell. The fine cell improved the properties of the composites [50].

Metals often react with carbon to form carbide, such as:

$$\frac{x}{y}M + C = \frac{1}{y}M_xC_y$$

when the reaction temperature reached 500 °C, aluminum react with graphite to form Al_4C_3. The specific surface area of graphene is large, the existing σ bonding between the in-plane carbon atoms in graphene leads to exceptionally stable and high mechanical properties. The σ bond formation can promote the formation of carbides. Because the graphene's basal plane is stable, the carbide formation is less influenced by the side contact. The contact interaction, through σ bond formation, tends to strongly result in the formation of Al_4C_3 at the interface, as confirmed by XRD (Fig. 10) and HRTEM (Fig. 11). However, there was less Al_4C_3. Hu et al. reported that excessive Al_4C_3 decreased the properties of composites. However, a certain amount Al_4C_3 can improve the wettability of graphene and Al, and thereby improves the properties of composites [38].

Fig. 16 shows the HRTEM microstructures of graphene and an alloy matrix. There was no obvious atomic vacancy at the interface between them (Fig. 16), indicating that there was a lower strain energy in the interface, and the interface was more stable. The nucleation and growth of microcracks were not easy to occur during the deformation, suggesting that Al-coated graphene/AlSi10Mg composites exhibited perfect mechanical properties. Moreover, graphene with high strength and high modulus of elasticity was homogeneously distributed within the matrix (Fig. 12), graphene was observed in the grain and near grain boundary (Fig. 17a). During the deformation process, the load could be effectively transferred from the metal matrix to graphene, and graphene could pin the grain boundaries and dislocations, lots of dislocation were aggregated near graphene, as shown in Fig. 17b, and thus increased the strength [51–53]. This strengthening phenomena were also observed in the polymer and ceramic nanocomposites [54–57]. Considering different thermal expansion coefficients of graphene and Al matrix, the thermal mismatch residual stress occurred near the interface between these two during the deformation process, which increased the dislocation density and led to work-hardening, and increased the strength of the composite material [1,26,58].

4. Conclusions

The aluminum coating was introduced on the graphene surface through a chemical reduction of organic aluminum, via nucleated and growth process. There were two primary grain growth patterns: two dimensional (2D) layered growth and three dimensional (3D) island growth during coating Al process. The Al-coated graphene was added into the AlSi10Mg alloy, refined the cell, and increased the tensile strength, hardness and wear resistance of the alloy. Coating of Al on the surface of graphene improved the wetting between graphene and Al, such that the addition of Al-coated graphene led to a high nucleation rate, and consequently the formation of fine cell. This approach facilitated the homogeneous distribution of graphene in the AlSi10Mg alloy, the interface between graphene and Al was relatively stable. These attributes contributed to the superior mechanical properties in the obtained AlSi10Mg alloy nanocomposites. Compared with polymers, carbon, ceramics and their nanocomposites [59–66] with the low thermal stability and relatively low electrical conductivity, the obtained

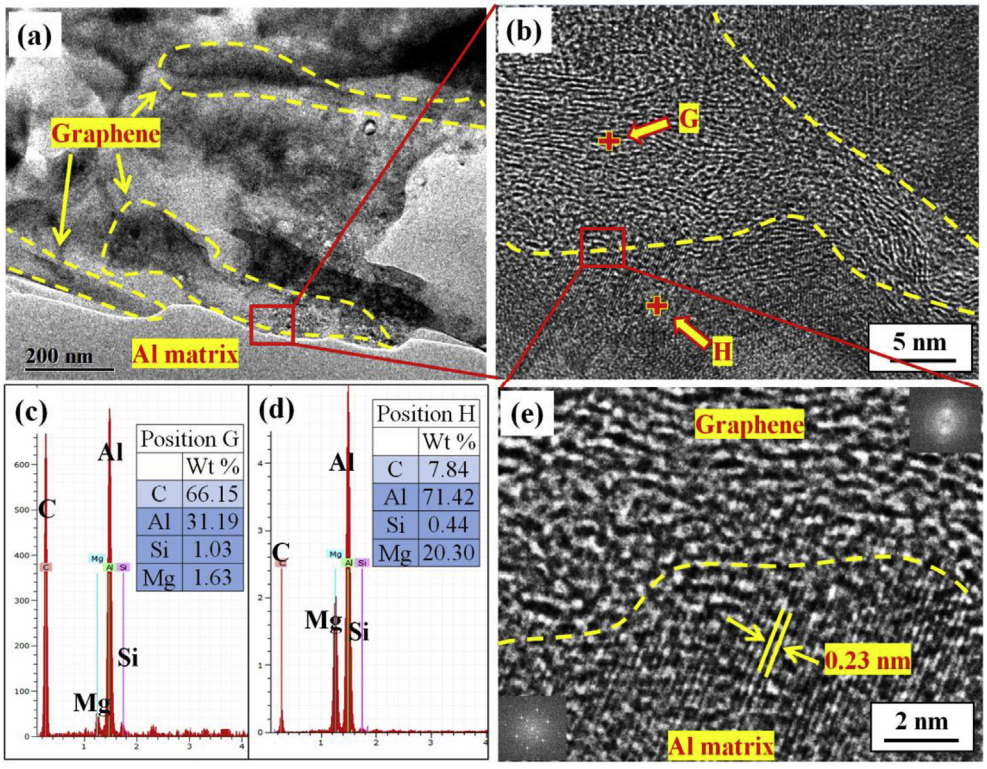

Fig. 16. High-resolution TEM microstrucures of (a, b and e) Al-coated graphene/AlSi10Mg composites, (c, d) composition analysis at point G and H.

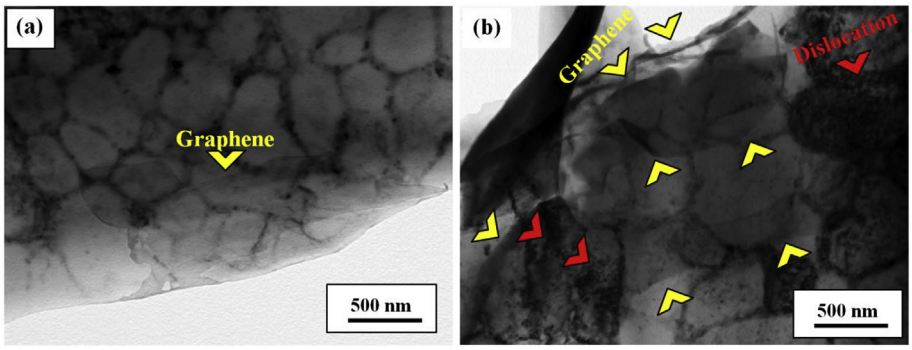

Fig. 17. TEM microstructures of Al-coated graphene/AlSi10Mg composites prepared by SLM: (a) before deformation, (b) after deformation.

metal-graphene nanocomposites can have many other applications where high electrical conductivity and thermal stability [67–70] are required.

Acknowledgements

The authors thank National Natural Science Foundation of China (Grant No. 51604246 and 51775521), Natural Science Foundation of Shanxi Province(Grant No. 201801D221154), the Major Science and Technology Projects of Shanxi Province, China (No. 20181101009) and the support of North University of China for Young Academic Leaders.

References

[1] W. Yang, Q. Zhao, L. Xin, et al., Microstructure and mechanical properties of graphene nanoplates reinforced pure Al matrix composites prepared by pressure infiltration method, J. Alloys Compd. 732 (2018) 748–758.
[2] Y. He, Q. Chen, S. Yang, et al., Micro-crack behavior of carbon fiber reinforced Fe_3O_4/graphene oxide modified epoxy composites for cryogenic application, Composites, Part A 108 (2018) 12–22.
[3] W. Xie, X. Zhu, S. Xu, et al., Cost-effective fabrication of graphene-like nanosheets from natural microcrystalline graphite minerals by liquid oxidation–reduction method, RSC Adv. 7 (2017) 32008–32019.
[4] B. Kirubasankar, V. Murugadoss, J. Lin, et al., In situ grown nickel selenide on graphene nanohybrid electrodes for high energy density asymmetric supercapacitors, Nanoscale 10 (2018) 20414–20425.
[5] M. Idrees, S. Batool, J. Kong, et al., Polyborosilazane derived ceramics - nitrogen sulfur dual doped graphene nanocomposite anode for enhanced lithium ion batteries, Electrochim. Acta 296 (2019) 925–937.
[6] W. Du, X. Wang, J. Zhan, et al., Biological cell template synthesis of nitrogen-doped porous hollow carbon spheres/MnO_2 composites for high-performance asymmetric supercapacitors, Electrochim. Acta 296 (2019) 907–915.
[7] K. Le, Z. Wang, F. Wang, et al., Sandwich-like NiCo layered double hydroxides/reduced graphene oxide nanocomposite cathode for high energy density asymmetric supercapacitors, Dalton Trans. (2019), https://doi.org/10.1039/C9DT00615J in press.
[8] W. Deng, T. Kang, H. Liu, et al., Potassium hydroxide activated and nitrogen doped graphene with enhanced supercapacitive behavior, Sci. Adv. Mater. 10 (2018) 937–949.
[9] M. Liu, Q. Meng, Z. Yang, X. Zhao, T. Liu, Ultra-long-term cycling stability of an integrated carbon–sulfur membrane with dual shuttle-inhibiting layers of graphene "nets" and a porous carbon skin, Chem. Commun. 54 (2018) 5090–5093.
[10] C. Wang, V. Murugadoss, J. Kong, et al., Overview of carbon nanostructures and nanocomposites for electromagnetic wave shielding, Carbon 140 (2018) 696–733.
[11] D. Jiang, V. Murugadoss, Y. Wang, et al., Electromagnetic interference shielding polymers and nanocomposites-A review, Polym. Rev. (2019), https://doi.org/10.1080/15583724.2018.1546737 in press.
[12] H. Qi, M. Teng, M. Liu, et al., Biomass-derived nitrogen-doped carbon quantum dots: highly selective fluorescent probe for detecting Fe3+ ions and tetracyclines, J. Colloid Interface Sci. 539 (2019) 332–341.
[13] H. Liu, Q. Li, S. Zhang, et al., Electrically conductive polymer composites for smart flexible strain sensors: a critical review, J. Mater. Chem. C 6 (2018) 12121–12141.
[14] H. Wei, H. Wang, Y. Xia, et al., An overview of lead-free piezoelectric materials and devices, J. Mater. Chem. C 6 (2018) 12446–12467.
[15] Y. Hu, Q. Guo, L. Zhao, et al., Correlating micro-pillar compression behavior with bulk mechanical properties: nanolaminated graphene-Al composite as a case study, Scripta Mater. 146 (2018) 236–240.
[16] Y. Zhao, X. Tian, B. Zhao, et al., Precipitation sequence of middle Al concentration alloy using the inversion algorithm and microscopic phase field model, Sci. Adv. Mater. 10 (2018) 1793–1804.
[17] Y. Zhao, L. Qi, Y. Jin, K. Wang, J. Tian, P. Han, The structural, elastic, electronic properties and Debye temperature of D022-Ni3V under pressure from first-principles, J Alloys Compd. 647 (2015) 1104–1110.
[18] R. Guan, C. Lian, Z. Zhao, R. Chao, C. Liu, Study on preparation of graphene and Al-graphene composite, Rare Metal Mater. Eng. 41 (2012) 607–611.
[19] Z. Zhao, R. Guan, J. Zhang, Z. Zhao, P. Bai, Effects of process parameters of semisolid stirring on microstructure of Mg-3Sn-1Mn-3SiC (wt%) strip processed by rheo-rolling, Acta Metall. Sin. 30 (2017) 66–72.
[20] Z. Zhao, P. Bai, R. Guan, et al., Microstructural evolution and mechanical strengthening mechanism of Mg-3Sn-1Mn-1La alloy after heat treatments, Mater. Sci. Eng. A 734 (2018) 200–209.
[21] C. Jeon, Y. Jeong, J. Seo, H. Tien, S. Hong, Y. Yum, S. Hur, K. Lee, Material properties of graphene/aluminum metal matrix composites fabricated by friction stir processing, Int. J. Precis. Eng. Manuf. 15 (2014) 1235–1239.
[22] H. Zhang, C. Xu, W. Xiao, K. Ameyama, C. Ma, Enhanced mechanical properties of Al5083 alloy with graphene nanoplates prepared by ball milling and hot extrusion, Mater. Sci. Eng. A 658 (2016) 8–15.
[23] J. Li, Y. Xiong, X. Wang, S. Yan, C. Yang, W. He, J. Chen, S. Wang, X. Zhang, S. Dai, Microstructure and tensile properties of bulk nanostructured aluminum/graphene composites prepared via cryomilling, Mater. Sci. Eng. A 626 (2015) 400–405.
[24] S. Yan, S. Dai, X. Zhang, C. Yang, Q. Hong, J. Chen, Z. Lin, Investigating aluminum alloy reinforced by graphene nanoflakes, Mater. Sci. Eng. A 612 (2014) 440–444.
[25] H. Asgharzadeh, M. Sedigh, Synthesis and mechanical properties of Al matrix composites reinforced with few-layer graphene and graphene oxide, J. Alloys Compd. 728 (2017) 47–62.
[26] J. Ju, G. Wang, K. Sim, Facile synthesis of graphene reinforced Al matrix composites with improved dispersion of graphene and enhanced mechanical properties, J Alloys Compd. 704 (2017) 585–592.
[27] F. Khodabakhshi, S. Arab, P. Svec, A. Gerlich, Fabrication of a new Al-Mg/graphene nanocomposite by multi-pass friction-stir processing: dispersion, microstructure, stability, and strengthening, Mater. Char. 132 (2017) 92–107.
[28] A. Rad, Adsorption of mercaptopyridine on the surface of Al- and B-doped graphenes: theoretical study, J. Alloys Compd. 682 (2016) 345–351.
[29] J.R. Croteau, S. Griffiths, M.D. Rossell, C. Leinenbach, C. Kenel, V. Jansen, D.N. Seidman, D.C. Dunand, N.Q. Vo, Microstructure and mechanical properties of Al-Mg-Zr alloys processed by selective laser melting, Acta Mater. 153 (2018) 35–44.
[30] S. Saedi, N.S. Moghaddam, A. Amerinatanzi, M. Elahinia, H.E. Karaca, On the effects of selective laser melting process parameters on microstructure and thermomechanical response of Ni-rich NiTi, Acta Mater. 144 (2018) 552–560.
[31] R. Li, P. Niu, T. Yuan, P. Cao, C. Chen, K. Zhou, Selective laser melting of an equiatomic CoCrFeMnNi high-entropy alloy: processability, non-equilibrium microstructure and mechanical property, J. Alloys Compd. 746 (2018) 125–134.
[32] Z. Zhao, J. Li, P. Bai, H. Qu, M. Liang, H. Liao, L. Wu, P. Huo, H. Liu, J. Zhang, Microstructure and mechanical properties of TiC-reinforced 316L stainless steel composites fabricated using selective laser melting, Metals 9 (2019) 267.
[33] Y. Zhao, B. Zhang, H. Hou, W. Chen, M. Wang, Phase-field simulation for the evolution of solid/liquid interface front in directional solidification process, J. Mater. Sci. Technol. 35 (2019) 1044–1052.
[34] B. Song, Z. Wang, Q. Yan, Y. Zhang, J. Zhang, C. Cai, Q. Wei, Y. Shi, Integral method of preparation and fabrication of metal matrix composite: selective laser melting of in-situ nano/submicro-sized carbides reinforced iron matrix composites, Mater. Sci. Eng. A 707 (2017) 478–487.
[35] A. Simchi, H. Pohl, Direct laser sintering of iron–graphite powder mixture, Mater. Sci. Eng. A 383 (2004) 191–200.
[36] H. Attar, L. Löber, A. Funk, M. Calin, L.C. Zhang, K.G. Prashanth, S. Scudino,

Y.S. Zhang, J. Eckert, Mechanical behavior of porous commercially pure Ti and Ti–TiB composite materials manufactured by selective laser melting, Mater. Sci. Eng. A 625 (2015) 350–356.
[37] D. Gu, Y.C. Hagedorn, W. Meiners, K. Wissenbach, R. Poprawe, Nanocrystalline TiC reinforced Ti matrix bulk-form nanocomposites by selective laser melting (SLM): densification, growth mechanism and wear behavior, Compos. Sci. Technol. 71 (2011) 1612–1620.
[38] Z. Hu, F. Chen, J. Xu, Q. Nian, D. Lin, C. Chen, X. Zhu, Y. Chen, M. Zhang, 3D printing graphene-aluminum nanocomposites, J. Alloys Compd. 746 (2018) 269–276.
[39] P. Sun, Z.Z. Fang, Y. Zhang, Y. Xia, Review of the methods for production of spherical Ti and Ti alloy powder, JOM 69 (2017) 1853–1860.
[40] R. Muszynski, B. Seger, P.V. Kamat, Decorating graphene sheets with gold nanoparticles, J. Phys. Chem. C 112 (2008) 5263–5266.
[41] W. Hong, H. Bai, Y. Xu, Z. Yao, Z. Gu, G. Shi, Preparation of gold nanoparticle/graphene composites with controlled weight contents and their application in biosensors, J. Phys. Chem. C 114 (2010) 1822–1826.
[42] J. Luo, S. Jiang, H. Zhang, J. Jiang, X. Liu, A novel non-enzymatic glucose sensor based on Cu nanoparticle modified graphene sheets electrode, Anal. Chim. Acta 709 (2012) 47–53.
[43] R. Jiang, X. Zhou, Z. Liu, Electroless Ni-plated graphene for tensile strength enhancement of copper, Mater. Sci. Eng. A 679 (2017) 323–328.
[44] W. Leng, H. Michael Barnes, Q. Yan, Z. Cai, J. Zhang, Low temperature synthesis of graphene-encapsulated copper nanoparticles from kraft lignin, Mater. Lett. 185 (2016) 131–134.
[45] Z. Zhao, R.D.K. Misra, P. Bai, J. Gao, Y. Li, R. Guan, Z. Guo, H. Liu, Novel process of coating Al on graphene involving organic aluminum accompanying microstructure evolution, Mater. Lett. 232 (2018) 202–205.
[46] Z. Zhao, P. Bai, L. Li, J. Li, L. Wu, P. Huo, L. Tan, The reaction thermodynamics during plating Al on graphene process, Materials 12 (2019) 330.
[47] S. Pal, N. Gubeljak, R. Hudak, G. Lojen, V. Rajtukova, J. Predan, V. Kokol, I. Drstvensek, Tensile properties of selective laser melting products affected by building orientation and energy density, Mater. Sci. Eng. A 743 (2019) 637–647.
[48] X. Li, X. Wang, M. Saunders, A. Suvorova, L. Zhang, Y. Liu, M. Fang, Z. Huang, T.B. Sercombe, A selective laser melting and solution heat treatment refined Al–12Si alloy with a controllable ultrafine eutectic microstructure and 25% tensile ductility, Acta Mater. 95 (2015) 74–82.
[49] X. Li, G. Ji, Z. Chen, A. Addad, Y. Wu, H. Wang, J. Vleugels, J. Van Humbeeck, J.P. Kruth, Selective laser melting of nano-TiB_2 decorated AlSi10Mg alloy with high fracture strength and ductility, Acta Mater. 129 (2017) 183–193.
[50] B. AlMangour, M.S. Baek, D. Grzesiak, K.A. Lee, Strengthening of stainless steel by titanium carbide addition and grain refinement during selective laser melting, Mater. Sci. Eng. A 712 (2018) 812–818.
[51] K. Chu, X. Wang, Y. Li, D. Huang, Z. Geng, X. Zhao, H. Liu, H. Zhang, Thermal properties of graphene/metal composites with aligned graphene, Mater. Des. 140 (2018) 85–94.
[52] D. Lin, M. Motlag, M. Saei, S. Jin, R.M. Rahimi, D. Bahr, G.J. Cheng, Shock engineering the additive manufactured graphene-metal nanocomposite with high density nanotwins and dislocations for ultra-stable mechanical properties, Acta Mater. 150 (2018) 360–372.
[53] Y. Mai, F. Chen, W. Lian, L. Zhang, C. Liu, X. Jie, Preparation and tribological behavior of copper matrix composites reinforced with nickel nanoparticles anchored graphene nanosheets, J. Alloys Compd. 756 (2018) 1–7.
[54] L. Ma, Y. Zhu, M. Wang, X. Yang, G. Song, Y. Huang, Enhancing interfacial strength of epoxy resin composites via evolving hyperbranched amino-terminated POSS on carbon fiber surface, Compos. Sci. Technol. 170 (2019) 148–156.
[55] L. Ma, N. Li, G. Wu, G. Song, X. Li, P. Han, G. Wang, Y. Huang, Interfacial enhancement of carbon fiber composites by growing TiO_2 nanowires onto amine-based functionalized carbon fiber surface in supercritical water, Appl. Surf. Sci. 433 (2018) 560–567.
[56] X. Li, S. Zhao, W. Hu, X. Zhang, L. Pei, Z. Wang, Robust superhydrophobic surface with excellent adhesive properties based on benzoxazine/epoxy/mesoporous SiO_2, Appl. Surf. Sci. 481 (2019) 374–378.
[57] H. Zhu, W. Hu, Y. Xu, B. Wang, D. Zheng, Y. Fu, C. Zhang, G. Zhao, Z. Wang, Gradient structure based dual-robust superhydrophobic surfaces with high-adhesive force, Appl. Surf. Sci. 463 (2019) 427–434.
[58] M. Li, H. Gao, J. Liang, S. Gu, W. You, D. Shu, J. Wang, B. Sun, Microstructure evolution and properties of graphene nanoplatelets reinforced aluminum matrix composites, Mater. Char. 140 (2018) 172–178.
[59] H. Gu, X. Xu, M. Dong, et al., Carbon nanospheres induced high negative permittivity in nanosilver-polydopamine metacomposites, Carbon 147 (2019) 550–558.
[60] H. Du, C.X. Zhao, J. Lin, et al., Carbon nanomaterials in direct liquid fuel cells, Chem. Rec. 18 (2018) 1365–1372.
[61] H. Sun, Z. Yang, Y. Pu, et al., Zinc oxide/vanadium pentoxide heterostructures with enhanced day-night antibacterial activities, J. Colloid Interface Sci. 547 (2019) 40–49.
[62] Z. Lin, B. Lin, Z. Wang, et al., Facile preparation of 1T/2H-Mo(S1-xSex)2 nanoparticles for boosting hydrogen evolution reaction, ChemCatChem (2019), https://doi.org/10.1002/cctc.201900095 in press.
[63] R. Ge, X. Ren, X. Ji, Z. Liu, G. Du, A. Asiri, X. Sun, L. Chen, Benzoate anions-intercalated layered cobalt hydroxide nanoarray: an efficient electrocatalyst for oxygen evolution reaction, ChemSusChem 10 (2017) 4004–4008.
[64] G. Zhu, X. Cui, Y. Zhang, et al., Poly (vinyl butyral)/graphene oxide/poly (methylhydrosiloxane) nanocomposite coating for improved aluminum alloy anticorrosion, Polymer (2019), https://doi.org/10.1016/j.polymer.2019.03.056 in press.
[65] Y. Sheng, J. Yang, F. Wang, et al., Sol-gel synthesized hexagonal boron nitride/titania nanocomposites with enhanced photocatalytic activity, Appl. Surf. Sci. 465 (2019) 154–163.
[66] R. Ge, S. Wang, J. Su, Y. Dong, Y. Lin, Q. Zhang, L. Chen, Phase-selective synthesis of self-supported RuP films for efficient hydrogen evolution electrocatalysis in alkaline media, Nanoscale 10 (2018) 13930–13935.
[67] F. Liu, Z. Xu, Z. Wang, et al., Structures and mechanical properties of Nb-Mo-Co(Ru) solid solutions for hydrogen permeation, J. Alloys Compd. 756 (2018) 26–32.
[68] H. Du, Y. An, Y. Wei, et al., Nickel powders modified nanocoating strengthened iron plates by surface mechanical attrition alloy and heat treatment, Sci. Adv. Mater. 10 (2018) 1063–1072.
[69] K. Engelkemeier, C. Nucke, K.P. Hoyer, M. Schaper, Anodizing of electrolytically galvanized steel surfaces for improved interface properties in fiber metal laminates, Adv. Compos. Hybrid Mater. 2 (2019) 189–199.
[70] R. Mishra, P. Sahay, R. Shahi, Alloying, magnetic and corrosion behavior of AlCrFeMnNiTi high entropy alloy, J. Mater. Sci. 54 (2019) 4433–4443.